THE AMERICAN SOCIETY OF MECHANICAL ENGINEERS
345 E. 47 St., New York, N.Y. 10017

82-GT-223

Comparison of Beam and Shell Theories for the Vibrations of Thin Turbomachinery Blades

A. W. Leissa
Professor,
Department of Engineering Mechanics,
Ohio State University

M. S. Ewing
Asst. Prof., Department of Engineering Mechanics,
United States Air Force Academy

A great deal of published literature exists which analyzes the free vibrations of turbomachinery blades by means of one-dimensional beam theories. Recently, a more accurate, two-dimensional analysis method has been developed based upon shallow shell theory. The present paper summarizes the two types of theories and makes quantitative comparisons of frequencies obtained by them. Numerical results are presented for cambered and/or twisted blades of uniform thickness. Significant differences between the theories are found to occur, especially for low aspect ratio blades. The causes of these differences are discussed.

INTRODUCTION

Vibration analysis of turbomachinery blades has traditionally been carried out by means of beam theory. One can find literally hundreds of references in the literature incorporating considerations such as coupling between bending and torsion, taper, shear deformation, rotary inertia, pretwist and rotational effects into one-dimensional beam vibration analyses. For example, a recent literature survey [1] uncovered approximately 150 references dealing with rotational effects in beam vibration analysis. Particularly notable among the carefully developed beam theories are those presented by Carnegie [2-8], Houbolt and Brooks [9] and Montoya [10]; these incorporate most of the considerations needed in blade vibration analysis by means of beam models and are widely used.

However, beam analysis becomes inadequate for low aspect ratio blades. Most obviously, vibration modes which involve predominantly chordwise bending are completely missed. These modes become more important as blade thicknesses and aspect ratios decrease. Furthermore, another important question arises: "Even for those modes obtainable from beam analysis (i.e., spanwise bending and torsion), how accurate is beam theory for low aspect ratio blades?"

In recent years two-dimensional methods of blade vibration analysis have been developed. As seen in a recent survey article [11], most of these utilize finite elements and tend to require considerable computation time. However, the chordwise bending effects are accounted for and, with properly conformable finite elements, accurate results are obtainable if sufficient elements are employed.

More recently a two-dimensional method of blade analysis has evolved which does not require finite elements and is based upon shell equations [12-14]. The method assumes general forms for the three components of displacement of a cantilever shell in terms of continuous functions, and utilizes the well known Ritz method to obtain frequencies and mode shapes. The method has been demonstrated to be computationally more efficient than finite elements [12] for the blade configurations that it can accomodate, and is well suited for parametric studies. It is also capable of providing very accurate solutions against which one-dimensional, beam model results can be compared.

The primary purpose of the present paper is to demonstrate the accuracy and limitations of blade vibration analyses which utilize one-dimensional, beam theories. From the thorough literature search previously performed by the senior author, it appears that no quantitative comparisons between the one-dimensional and the more accurate two-dimensional models have been previously undertaken. Furthermore, where the results of beam analysis have been compared with experiment, it has only been for blades of relatively large aspect ratio. For this reason the present work makes comparisons between the theories and experiment for low aspect ratios as well. Of particular importance are the effects of shear deformation, rotary inertia and warping which should be properly dealt with

Contributed by the Gas Turbine Division of the ASME.

by beam models, and which can become more significant for smaller aspect ratios.

In the two sections which follow the essential descriptions of the beam theory and shell theory to be used in subsequent comparisons are laid out. Each section has its own notation, independent of the other, consistent with widespread usage in beam and shell theory and following closely the notation used in the relevant references. In subsequent sections quantitative comparisons of vibration frequencies obtained from beam theory and shell theory are made for blades having camber and/or twist. Models are chosen for which other accurate analyses can also be found in the published literature. Finally, a concluding section summarizes the limitations of beam theory and what is needed to make it more accurate for the spanwise bending and torsional modes which it may reasonably represent.

BEAM THEORY DESCRIPTION

Undoubtedly the most thorough work to develop a comprehensive set of equations representing a vibrating blade as a beam was presented in a sequence of papers by Carnegie [2-8] which appeared during the period 1957-1967. In the first work [2] potential energy functionals were derived for a twisted blade of arbitrary cross-section, and variational methods were then employed to obtain static equations of equilibrium describing bending about two axes and torsion. These equations were then integrated for the case of cross-sections uniform along the length subjected to either concentrated or uniformly distributed transverse static loadings, and numerical results were obtained for blades of rectangular and airfoil cross-sections.

Vibrations were taken up in a subsequent paper [3]. The strain energy of elastic deformation used in the static analysis [2] was taken, i.e.,

$$V = \frac{1}{2}\int_0^l \left\{ EI_{yy}\left(\frac{\partial^2 u}{\partial z^2}\right)^2 + 2EI_{xy}\frac{\partial^2 u}{\partial z^2}\frac{\partial^2 v}{\partial z^2} + EI_{xx}\left(\frac{\partial^2 v}{\partial z^2}\right)^2 + C\left(\frac{\partial \theta}{\partial z}\right)^2 \right\} dz \qquad (1)$$

and the kinetic energy was written as

$$T = \frac{1}{2}\int_0^l \left\{ \rho\left(\dot{u} + r_y\dot{\theta}\right)^2 + \rho\left(\dot{v} + r_x\dot{\theta}\right)^2 + I_c\dot{\theta}^2 \right\} dz \qquad (2)$$

where z is the longitudinal (i.e., spanwise) coordinate passing through the centers of flexure (see Fig. 1) of the cross-sections, x and y are coordinates orthogonal to z, and u and v are displacements in the x and y directions, respectively. Figure 1 also shows an XYZ coordinate system, with Z being parallel to z and passing through the centroid of the blade cross-section, and X and Y being the axes of principal moments of inertia I_{xx} and I_{yy} (more properly, the principal second moments of areas). The moments and product of inertia I_{xx}, I_{yy} and I_{xy} are taken with respect to axes parallel to x and y and passing through the centroid. The angular displacement during torsional vibration is given by θ, and C is the torsional stiffness of the cross-section, ρ is mass per unit length and I_c is the polar mass moment of inertia per unit length with respect to the centroid. Time derivatives in Eq. 2 are denoted by dots above the variables. Applying the Euler-Lagrange equations of the calculus of variations yielded the equations of motion [3]

$$\frac{\partial^2}{\partial z^2}\left\{ EI_{yy}\frac{\partial^2 u}{\partial z^2} + EI_{xy}\frac{\partial^2 v}{\partial z^2} \right\} = -\rho\left(\ddot{u} + r_y\ddot{\theta}\right) \qquad (3a)$$

$$\frac{\partial^2}{\partial z^2}\left\{ EI_{xy}\frac{\partial^2 u}{\partial z^2} + EI_{xx}\frac{\partial^2 v}{\partial z^2} \right\} = -\rho\left(\ddot{v} + r_x\ddot{\theta}\right) \qquad (3b)$$

$$\frac{\partial}{\partial z}\left(C\frac{\partial \theta}{\partial z}\right) = \rho r_y\ddot{u} + \rho r_x\ddot{v} + \left(\rho r_y^2 + \rho r_x^2 + I_c\right)\ddot{\theta} \qquad (3c)$$

Eqs. (3) show clearly the coupling which exists between the three displacement variables u, v and θ. For a general section possessing no symmetry (such as in Fig. 1), coupling is complete among the two bending displacements and the torsional displacement.

Another significant contribution of Carnegie's second paper [3] was the recognition of additional torsional stiffness in a cantilevered blade beyond that represented by C. In the case of a straight blade the constant C depends upon the cross-sectional shape and the shear modulus (G), and is determined by solving the St. Venant torsion problem of classical elasticity for the given shape (cf. [15], Chapter 10). But the St. Venant torsion problem assumes that both ends of the blade are free to warp out of their xy-planes. Clearly, the clamped end of a cantilevered blade is restrained from warping, and this constraint yields additional torsional stiffness to the blade. Carnegie [3] viewed the additional stiffness as being due to "torsion bending" - that is, the additional stiffness due to the longitudinal fibers each being bent as cantilever beams during the torsional rotations of the cross-sections. For a straight blade of rectangular cross-section having width b and depth h, he showed that the total twisting

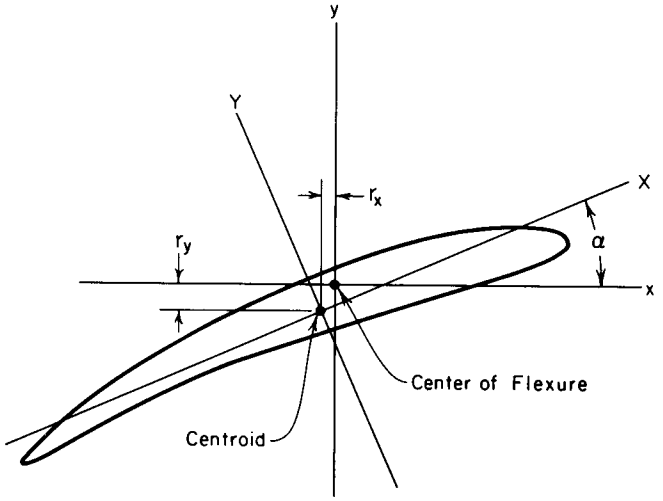

Figure 1 Typical blade cross-section, showing coordinates for beam analysis.

moment at a typical location (z) is given by

$$M_\theta = C\frac{\partial\theta}{\partial z} - C_1\frac{\partial^3\theta}{\partial z^3} \qquad (4)$$

where $C = Gbh^3/3 = Ebh^3/6(1+\nu)$ is the St. Venant torsional stiffness constant, and

$$C_1 = Eb^3h^3/144 \qquad (4')$$

Of course, the second term of Eq. (4) causes additional stiffening in spite of the negative sign because, at a point having $\partial\theta/\partial z$ positive, $\partial^3\theta/\partial z^3$ is typically negative. The correction factor C_1 was shown to have little effect upon the fundamental torsional frequency of a typical, large aspect ratio blade, but to have pronounced effect upon the higher torsional frequencies ([3], Figs. 11 and 15).

The additional torsional stiffening was expounded upon further in a subsequent publication [5]. Therein Carnegie demonstrated that the torsional strain energy term (last term in Eq. (1)) is generalized to

$$C\left(\frac{\partial\theta}{\partial z}\right)^2 - C_1\frac{\partial\theta}{\partial z}\frac{\partial^3\theta}{\partial z^3} \qquad (5)$$

and that the third equation of motion (3c) has its left-hand-side replaced by

$$\frac{\partial}{\partial z}\left(C\frac{\partial\theta}{\partial z} - C_1\frac{\partial^3\theta}{\partial z^3}\right) \qquad (6)$$

and the order of the system of differential equations (3) is thereby raised from ten to twelve. The latter set requires the statement of six boundary conditions at each end of the blade; in particular, for the cantilever blade of length ℓ,

$$u = \frac{\partial u}{\partial z} = v = \frac{\partial v}{\partial z} = \theta = \frac{\partial\theta}{\partial z} = 0, \text{ at } z=0 \qquad (7a)$$

$$M_x = M_y = Q_x = Q_y = \frac{\partial\theta}{\partial z^2} = M_\theta = 0, \text{ at } z=\ell \qquad (7b)$$

where M_x and M_y are the bending moments about the x and y axes, Q_x and Q_y are the transverse shearing forces in the x and y directions and M_θ is the twisting moment, given by Eq. (4).

In an interesting discussion of the Carnegie paper, Barr pointed out (see [5], p. 319) that the additional torsional stiffness constant C_1 could be obtained from the classical St. Venant torsion theory by solving for the warping function ψ, where the longitudinal (z-direction) displacement w determines the warping, and is given by

$$w(x,y) = \psi(x,y)\frac{\partial\theta}{\partial z} \qquad (8)$$

and the constant C_1 is then obtained from

$$C_1 = E\iint\psi^2\,dx\,dy \qquad (9)$$

As part of his reply to Barr's discussion, Carnegie also showed that the torsional strain energy term (5) can be equivalently written as

$$C\left(\frac{\partial\theta}{\partial z}\right)^2 + C_1\left(\frac{\partial^2\theta}{\partial z^2}\right)^2 \qquad (10)$$

Carnegie [6] also added the effects of shear deformation and rotary inertia to the problem, following the now well-known approach first suggested by Timoshenko [16]. In considering shear deformation the changes in slope of a beam due to bending and shear must be entered into the problem independently, and the strain energy functional (1) is generalized to

$$V = \frac{1}{2}\int_0^\ell\left\{EI_{xx}\left(\frac{\partial\phi_x}{\partial z}\right)^2 + 2EI_{xy}\frac{\partial\phi_x}{\partial z}\frac{\partial\phi_y}{\partial z} + EI_{yy}\left(\frac{\partial\phi_y}{\partial z}\right)^2 + \frac{AG}{2k}\left[\left(\frac{\partial u}{\partial z}-\phi_x\right)^2+\left(\frac{\partial v}{\partial z}-\phi_y\right)^2\right] + C\left(\frac{\partial\theta}{\partial z}\right)^2 + C_1\left(\frac{\partial^2\theta}{\partial z^2}\right)^2\right\}dz \qquad (11)$$

where, for example, the shearing slope in the xz-plane, $\partial u/\partial z - \phi_x$, is the difference between the total slope ($\partial u/\partial z$) and the slope due to bending alone (ϕ_x). The shear rigidity also involves the blade cross-sectional area (A), and a shear stress distribution factor (k) depending upon cross-sectional shape. The kinetic energy functional is given by Eq. (2) with the terms reflecting the rotary inertia [7] added to the integrand:

$$\rho\left[\dot\phi_x + \frac{\partial}{\partial z}(r_y\dot\theta)\right]^2 + \rho\left[\dot\phi_y + \frac{\partial}{\partial z}(r_x\dot\theta)\right]^2 \qquad (12)$$

During the foregoing theoretical development, the dynamic effects due to blade rotation while mounted on a disk were added to the problem [4], including both the stabilizing (frequency increasing) primary and the destabilizing (frequency decreasing) secondary centrifugal force effects. The final, most general potential and kinetic energy functions, along with corresponding equations of motion, were summarized in a short note [7] in 1966. Experimental studies [2, 3, 17, 18] were also made, which verified most of the theoretical conclusions.

Where numerical solutions were given in the papers by Carnegie described above, they were obtained in a few cases by exact integration of the equations of motion, but more often by a somewhat crude Rayleigh method using static deflection functions to represent the mode shapes. Subsequent papers with colleagues (for example, [19-23]) served to obtain more accurate solutions by other approximate methods such as finite differences, Runge-Kutta numerical integration, Ritz-Galerkin, and an extended Holzer technique. Most of these publications are summarized in survey papers by one of the present authors [1] and Rao [24-26]. By and large, the following general comments can be made about the references containing numerical results:

1. Blades are of large aspect ratio
2. Airfoil cross-sectional data is not given, thereby preventing comparison by other methods.
3. The torsional warping constant C_1 is not considered.

Houbolt and Brooks [9] and Montoya [10] also derived sets of differential equations of motion for twisted blades of arbitrary cross-section. However, in both derivations neither shear deformation nor rotary inertia were included. Nor were the effects of cross-sectional warping during bending or cross-sectional warping constraint during torsion explicitly considered in either analysis.

In the present work beam theory representations of blades will be made by

means of Carnegie's equations which, as the foregoing paragraphs have indicated, appear to be the most comprehensive set thus far appearing in the published literature of blade vibrations. Although an exact solution of the twelfth order set of differential equations of motion is possible for the cantilevered blade, the procedure is algebraically cumbersome, and a straightforward Ritz procedure will be used instead. For the free vibration problem, classical beam theory displacements u, v, and θ are taken as

$$\begin{aligned} u(z,t) &= U(z)\sin\omega t \\ v(z,t) &= V(z)\sin\omega t \\ \theta(z,t) &= \Theta(z)\sin\omega t \end{aligned} \qquad (13)$$

where ω is the radial frequency. The functions U, V, and Θ must be chosen such that:

1. the geometric boundary conditions (7a) are exactly satisfied along the clamped edge,
2. the functions form complete sets (i.e., capable of representing any set of kinematically possible displacements along the blade axis).

For the present problem a set of displacements for straightforward application is given by the algebraic polynomials

$$U(z) = \sum_{i=1}^{I} A_i z^i, \quad V(z) = \sum_{j=1}^{J} B_j z^j, \quad W(z) = \sum_{k=2}^{K} C_k z^k,$$

$$\Phi_x(z) = \sum_{l=1}^{L} D_l z^l, \quad \Phi_y(z) = \sum_{m=1}^{M} E_m z^m \qquad (14)$$

when shear deformation and torsional warping constraint are now included. For the classical Euler-Bernoulli theory, the functions Φ_x and Φ_y are not used, and the index k begins at one, instead of two. To apply the Ritz method the functional $T_{max} - V_{max}$ is formed, where T_{max} and V_{max} are the maximum values of kinetic energy (i.e., at maximum velocity) and potential energy (i.e., at maximum displacement). The functional is then minimized by equations of the type

$$\frac{\partial(T_{max} - V_{max})}{\partial A_i} = 0, \quad (i = 1, 2 \cdots I) \qquad (15)$$

with derivatives taken with respect to each of the A_i, B_j, C_k, D_l, E_m in turn, and where V is given by Eq. (11) and T by Eq. (2) with the terms (12) added, yielding a set of $I+J+K+L+M-1$ simultaneous linear algebraic equations in the same number of unknowns $A_i, \cdots, E_m$. For a nontrivial solution the determinant of the coefficient matrix of the equations is set equal to zero and the roots of the determinant are the eigenvalues (i.e., nondimensional frequencies). The eigenfunctions (mode shapes) are determined by back-substitution of the eigenvalues in the usual way. The resulting frequencies are upper bounds on the exact frequencies and, if a complete set of functions such as Eqs. (14) is used, the exact beam frequencies can be determined as accurately as desired.

SHELL THEORY DESCRIPTION

The shell analysis used in this work is based upon shallow shell theory. This theory contains the essential features needed, namely, bending and stretching effects coupled together, and is applicable provided the curvature and twist are relatively small. It is capable of representing variable curvature and twist and variable thickness and, for blades which are relatively thick, can be generalized to include shear deformation and rotary inertia effects. However, the present study will be limited to blades which are sufficiently thin so that the latter effects can be neglected. For shells of arbitrary curvature and twist, deep shell theory will typically involve non-principal, nonorthogonal coordinates with considerable complication in the resulting equations (cf. [27], p. 54), and is therefore desirable to avoid in blade analysis.

Consider the simplified model of a rotating blade shown in Figure 2. It has a length a, a planform width b (i.e., the projected width in the xy reference plane) and a thickness h. The present study assumes a rectangular planform for the blade, although other shapes can also be treated. The blade is represented as a shallow shell having curvature $1/R_y$ in the y-direction. Twist ($1/R_{xy}$) is not shown, but can be readily accomodated in the analysis. The shell is assumed rigidly clamped at one end ($x = 0$), whereas the other three edges are completely free. Angular velocity Ω is assumed about an axis located at a hub radius r_o from the blade root. The blade is inclined with a stagger angle θ with respect to the rotation axis. Displacements are measured as in conventional shell theory by w taken normal to the shell midsurface, and u and v tangent to the midsurface, with u being parallel to the x-direction.

The present analysis utilizes the well-known Ritz method and is therefore based upon the potential and kinetic energy functionals. The total potential energy of the rotating shell can be written as

$$V = V_1 + V_2 + V_3 + V_4 \qquad (16)$$

where V_1 is the strain energy of stretching (cf., [27-29])

$$V_1 = \frac{Eh}{2(1-\nu^2)} \int_{-b/2}^{b/2} \int_0^a \left\{ (\epsilon_x + \epsilon_y)^2 - 2(1-\nu)\left[\epsilon_x \epsilon_y - \frac{\gamma_{xy}^2}{4} \right] \right\} dx\, dy \qquad (17)$$

and V_2 is the strain energy of bending

$$V_2 = \frac{Eh^3}{12(1-\nu^2)} \int_{-b/2}^{b/2} \int_0^a \left\{ (\nabla^2 w)^2 - 2(1-\nu)\left[\frac{\partial^2 w}{\partial x^2}\frac{\partial^2 w}{\partial y^2} - \left(\frac{\partial^2 w}{\partial x\, \partial y} \right)^2 \right] \right\} dx\, dy \qquad (18)$$

In the above expressions ϵ_x, ϵ_y and γ_{xy} are the membrane strains given by

$$\epsilon_x = \frac{\partial u}{\partial x} + \frac{w}{R_x}, \quad \epsilon_y = \frac{\partial v}{\partial y} + \frac{w}{R_y}$$

$$\gamma_{xy} = \left(\frac{\partial v}{\partial x} + \frac{\partial u}{\partial y} \right) + 2\frac{w}{R_{xy}} \qquad (19)$$

E is Young's modulus and ν is Poisson's ratio.

The functionals V_3 and V_4 are due to the centrifugal forces of rotation, with V_3 being due to the steady, radially directed components of body forces; that is,

$$V_3 = \frac{1}{2}\int_{-b/2}^{b/2}\int_0^a \left\{ N_x^\circ \left(\frac{\partial w}{\partial x}\right)^2 + N_y^\circ \left(\frac{\partial w}{\partial y}\right)^2 + 2N_{xy}^\circ \frac{\partial w}{\partial x}\frac{\partial w}{\partial y} \right\} dx\,dy \qquad (20)$$

where N_x°, N_y°, and N_{xy}° are the membrane stress resultants (i.e., force per unit length) caused by the body forces. Finally, V_4 represents the potential of the displacement dependent body forces (i.e., components which exist because of vibratory displacements u, v and w), which is formulated in detail in Reference 12. The functional V_3 is caused predominantly by tensile stresses, and increases the vibration frequencies, whereas V_4 is caused mainly by normal body forces in the direction of positive w, and typically reduces the frequencies [12].

The kinetic energy of vibratory motion is

$$T = \frac{\rho h}{2}\int_{-b/2}^{b/2}\int_0^a (\dot{u}^2 + \dot{v}^2 + \dot{w}^2)\,dx\,dy \qquad (21)$$

where the dots denote time derivatives of the displacements and ρ is the mass per unit volume. Coriolis effects are neglected.

To solve the free vibration problem for the blade, a Ritz procedure is followed similar to that described in the previous section on beam theory. That is, one takes the vibratory displacements to be sinusoidal functions of time; i.e.,

$$\begin{aligned} u(x,y,t) &= U(x,y)\sin\omega t \\ v(x,y,t) &= V(x,y)\sin\omega t \\ w(x,y,t) &= W(x,y)\sin\omega t \end{aligned} \qquad (22)$$

where ω is the vibration frequency, and U, V and W are chosen to be the algebraic polynomials

$$U(x,y) = \sum_{i=1}^{I}\sum_{j=0}^{J} A_{ij}\,x^i y^j,\quad V(x,y) = \sum_{k=1}^{K}\sum_{l=0}^{L} B_{kl}\,x^k y^l,$$

$$W(x,y) = \sum_{m=2}^{M}\sum_{n=0}^{N} C_{mn}\,x^m y^n \qquad (23)$$

The functional $T_{max} - V_{max}$ is again formed and it is minimized by setting

$$\frac{\partial}{\partial A_{ij}}(T_{max} - V_{max}) = 0,\quad (i=1,\cdots,I;\ j=0,\cdots,J)$$

$$\frac{\partial}{\partial B_{kl}}(T_{max} - V_{max}) = 0,\quad (k=1,\cdots,K;\ l=0,\cdots,L)$$

$$\frac{\partial}{\partial C_{mn}}(T_{max} - V_{max}) = 0,\quad (\text{etc.}) \qquad (24)$$

yielding a set of $I(J+1) + K(L+1) + (M-1)(N+1)$ linear algebraic equations in the same number of unknowns, and a matrix eigenvalue problem of the same type as in the previously described beam analysis.

COMPARISONS FOR CAMBERED BLADES

Convergence studies were made for the beam theories, both including and neglecting shear deformation and rotary inertia, to establish the upper limits of the summations in Eqs. (14) required to obtain desired convergence. Cambered blade configurations as shown in Fig. 2 having a thickness ratio (b/h) of 20 were investigated, having various combinations of aspect ratio (a/b) and shallowness parameter (b/R). It was found that between six and ten terms of the polynomials were needed to yield convergence of the frequencies to four significant figures for the first four modes of each symmetry class, the number required depending upon the particular mode in question. For the cambered blade of Fig. 2, symmetry uncouples v and ϕ_y from u, ϕ_x and θ.

The accuracy of the beam equations and the computer programming, as well as the rate of convergence of the Ritz method with the algebraic polynomials, was also established by comparison with the numerical results obtained by Subrahmanyam, Kulkarni and Rao [30] for a particular blade (see Ref. 30, p. 20). Their results were also obtained by means of the Carnegie equations, but using slightly different displacement functions. Using seven terms for each of the polynomials (14) excellent agreement ($<0.1\%$ difference) was observed for each of the frequencies (5) found in Ref. 30.

A direct comparison of numerical results for the frequencies of cambered blades obtained from beam theory and shell theory is made in Table 1. The nondimensional frequency parameter used in Table 1 is $\omega a^2\sqrt{\rho h/D}$ which is a traditional one used for flat plates. Because the blade curvatures utilized in Table 1 are all quite shallow (the deepest curvature, $b/R = 0.5$, corresponds to a circular arc measure of 28.9°), the plate frequency parameter is appropriate.

All shear deformation theory results in Table 1 are for a thickness ratio $b/h = 20$ and a Poisson's ratio (ν) of 0.3. A shear correction factor $k = 1.2$ was used (note that this is the reciprocal of the factor often used in the published literature) which is

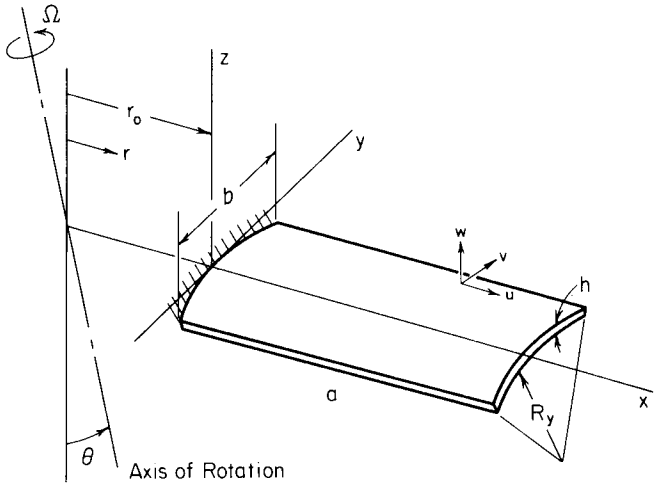

Fig. 2. Simplified model of a rotating blade.

Table 1. Comparison of $\omega a^2\sqrt{\rho h/D}$ Between Shell and Beam Theories for Cambered Blades ($b/h=20$)

$\frac{a}{b}$	$\frac{b}{R}$	Mode No.	Symmetric Modes			Antisymmetric Modes				
				Beam theory			Beam theory (no C_1)		Beam theory (with C_1)	
			Shell theory	Shear def. and R.I.	Classical	Shell theory	Shear def. & R.I.	Classical	Shear def. & R.I.	Classical
5	0.1	1	3.516	3.463	3.463	33.98	32.12	32.21	33.86	33.86
		2	21.95	21.69	21.70	65.35*	65.08*	67.11*	65.09*	67.11*
		3	61.62	60.68	60.76	103.9	96.38	96.64	103.5	103.5
		4	127.9	118.8	119.1	179.6	160.6	161.1	178.7	178.7
	0.3	1	4.271	4.242	4.242	34.00	31.90	31.99	33.63	33.63
		2	26.43	26.56	26.58	65.36*	65.33*	67.36*	65.35*	67.38*
		3	73.83	74.28	74.44	104.1	95.79	96.05	102.9	102.9
		4	148.3	145.3	145.9	180.2	159.6	160.0	177.6	177.7
	0.5	1	5.454	5.513	5.514	34.02	31.46	31.55	33.17	33.17
		2	33.51	34.50	34.55	65.37*	65.81*	67.87*	65.86*	67.91*
		3	92.48	96.41	96.75	104.3	94.61	94.88	101.7	101.7
		4	181.3	188.4	189.6	181.1	157.5	158.0	175.5	175.5
2	0.1	1	3.545	3.461	3.463	14.81	12.85	12.85	14.74	14.74
		2	21.92	21.62	21.70	48.23	38.55	38.65	48.04	48.04
		3	61.00	60.24	60.76	57.52*	57.08*	67.11*	57.11*	67.11*
		4	93.28†	———	———	92.67	64.25	64.42	91.91	91.91
	0.3	1	4.264	4.239	4.242	14.84	12.77	12.80	14.65	14.65
		2	25.25	26.44	26.58	48.39	38.30	38.41	47.76	47.78
		3	66.81	73.47	74.44	57.52*	57.28*	67.36*	57.33*	67.36*
		4	93.38	———	———	93.25	63.85	64.02	91.45	91.47
	0.5	1	5.398	5.506	5.514	14.89	12.60	12.64	14.47	14.48
		2	30.64	34.23	34.55	48.70	37.79	37.91	47.20	47.24
		3	76.51	94.67	96.75	57.54*	57.68*	67.86*	57.75*	67.86*
		4	93.54†	———	———	94.39	63.03	63.20	90.52	90.57
1	0.1	1	3.561	3.456	3.463	8.516	6.425	6.442	8.485	8.485
		2	21.48	21.39	21.70	31.00	19.28	19.33	30.94	30.94
		3	27.22†	———	———	43.56*	42.93*	67.11*	42.99*	67.11*
		4	54.28††	———	———	64.28**	———	———	———	———
	0.3	1	4.181	4.229	4.242	8.543	6.385	6.402	8.438	8.439
		2	22.76	26.01	26.58	31.17	19.15	19.21	30.77	30.79
		3	27.42†	———	———	43.56*	43.01*	67.35*	43.14*	67.35*
		4	54.52††	———	———	64.29**	———	———	———	———
	0.5	1	5.168	5.484	5.514	8.595	6.303	6.320	8.344	8.346
		2	24.66	33.33	34.55	31.50	18.90	18.96	30.45	30.50
		3	28.11†	———	———	43.57*	43.08*	67.83*	43.45*	67.82*
		4	55.03††	———	———	64.31**	———	———	———	———

† Chordwise bending mode

†† Combined mode

* Sideways bending mode

** Antisymmetric chordwise bending mode

representative of the cross-sections dealt with in this analysis. For comparison, setting $\lambda=\infty$ yields the classical theory results presented in Table 1, and setting $\lambda=1$ (which is the theoretical lower limit) was found to yield values of less than 0.1 percent different than those given in Table 1 for $\lambda=1.2$.

Numerical results according to shallow shell analysis are obtained using 54 degrees of freedom. This is arrived at from the algebraic polynomials (23) by choosing 6 terms in the α-direction (Fig. 2) and 3 terms of even degree in u and w, and odd degree in v in the y-direction for each of the displacements u, v, and w. These results are taken from a previous paper [13], and their convergence was demonstrated there.

Considering first the symmetric modes of the large aspect ratio ($a/b = 5$) blades in Table 1, one sees that the frequencies of the first three spanwise bending modes are in reasonably close agreement, although a significant difference between shell and beam theory results of as much as 7 percent occurs for the fourth spanwise bending mode. Of course, for higher modes, the differences would become greater. It is interesting to note that for $b/R = 0.1$, the frequencies predicted by shell theory are greater than those of beam theory, whereas for deeper blades the opposite is true. This may be explained as follows: For a flat (or nearly flat) plate, chordwise bending moments exist, which give the plate additional stiffness unrecognized by beam theory, whereas for deeper blades, warping effects begin to become more important.

Strong warping effects are seen to enter the results for the shorter aspect ratio blades, especially as the curvature increases. For $b/R = 0.5$, for example, and $a/b = 2$ and 1, the beam theories give results for the second bending mode frequencies which are 12 and 35 percent too high, respectively. This reflects the inability of the beam theories to permit cross-sectional warping. That is, the beam theory hypothesis that "plane cross-sections remain plane during beam deflection" can become significantly violated for small aspect ratio, cambered blades. Or in other words, shear lag effects yield a more flexible system than either beam theory recognizes.

Table 1 also shows that for moderate to low aspect ratios, certain important mode shapes are missed altogether by beam theory. For example, a mode with predominantly normal (w) displacement, and with the greatest curvature changes occuring in the chordwise direction (which we will term "chordwise bending"), is the fourth and third symmetric mode for $a/b = 2$ and 1, respectively, for all the curvatures given. For $a/b = 1$ and significant camber ($b/R = 0.3$ and 0.5) the fourth symmetric mode is a more complex one, also not found by the beam theories.

As an example, Fig. 3 depicts the symmetric mode shapes for the cambered blade having $b/h = 20$, $a/b = 1$, $b/R = 0.5$, corresponding to the last four shell frequency parameters given in Table 1.

Three sketches aligned in a horizontal row are given for each mode shape. The sketches show contour lines of equal displacement, normalized with respect to the maximum normal displacement; that is W/W_{max}, V/W_{max} and U/W_{max}, in this sequence. Although the W displacements are usually largest during vibration, at least for the lowest frequency modes, the magnitude of the tangential coupling due to U and V displacements can also be seen from the drawings. The contour lines correspond to normalized displacement increments of 0.1, with the lines of zero displacement (node lines) being drawn heavier.

For the short, highly cambered blade of Fig. 3 the first symmetric mode is clearly identifiable as spanwise bending. The second and third modes are mainly second spanwise bending and chordwise bending, respectively, although considerable coupling exists between them. This coupling causes the large differences between the second spanwise frequencies given in Table 1. The fourth mode is seen in Fig. 3 to be a combined one consisting of both chordwise and spanwise bending.

Table 1 also presents the nondimensional frequency parameters $\omega a^2\sqrt{\rho h/D}$ for the antisymmetric modes of the cambered blade. The antisymmetric modes involve coupling between sideways (y-direction) and torsional motions. The two last columns of the antisymmetric mode did not appear for the symmetric modes. They show the effect on the beam frequencies if a torsional warping constant C_1 (see Eq. 4) is added to the analysis. For the blade configurations in Table 1 having $a/b = 5$ and 2, the first four antisymmetric modes contain three modes which are predominantly torsional, whereas the remaining one is predominantly sideways bending, as indicated by asterisks. One notes that the torsional frequencies predicted by the classical beam theory are essentially the same as when shear deformation and rotary inertia are included, and would be exactly the same if it were not for a small amount of coupling. However, the beam theories give considerably different frequencies for the sideways bending modes, especially for small a/b, as one would expect to find when considering or neglecting shear deformation and rotary inertia effects. For $a/b = 1$ the fourth mode is antisymmetric chordwise bending, which the beam theory misses completely. In interpreting Table 1 one must bear in mind that changing a/b corresponds to changing b and keeping a fixed, if the changes in frequencies are to be observed, because the frequency parameter used contains a .

But the most important comparison of antisymmetric frequencies in Table 1 is between the torsional frequencies of shell theory and those of beam theory. If C_1 is not included, one sees large differences, again particularly for small a/b and for the higher modes. The shell theory torsional frequencies are essentially those of flat plates, only slightly affected by the changing cross-sectional arc length caused by changing b/R (b is kept fixed and R changed). These torsional frequencies agree with those readily available for flat plates in the literature (cf., [31,32]). Even for a large aspect ratio blade ($a/b = 5$), considerable differences ($\sim 10\%$) are seen to occur between shell and beam frequencies for the third (and higher) torsional modes, as was also found by Carnegie ([3], Figs. 11 and 15) when comparing beam theory frequencies with experimentally measured ones. For $a/b = 1$ the third torsional beam frequency in Table 1 is seen to differ from the more accurate shell frequency by about 50 percent.

However, when C_1 is included, the warping constraint is substantially accounted for, and the results of beam theory are seen to agree reasonably well with those of shell theory. In the present analysis the value of C_1 for a thin rectangle ($Eb^3h^3/144$) was

used because no proper value for the annular sector is currently known. For small camber however, the approximation as a rectangle should be very good.

The first four antisymmetric modes of the blade having $b/h = 20$, $a/b = 1$ and $b/R = 0.5$ (i.e., the same as for Fig. 3) are depicted by Fig. 4. For the first two modes, which are torsional, the contour lines for the W-displacement agree closely with those of the beam theories. The predominant sidewise bending of the third mode shape and the antisymmetric chordwise bending of the fourth are both clearly seen in Fig. 4.

COMPARISON FOR TWISTED BLADES

Table 2 makes comparisons among the numerical results obtained from the present shell theory, Carnegie's beam theory (including shear deformation and rotary inertia) and those of Petricone and Sisto [33] for a blade having twist only; that is, the curvatures $1/R_x$ and $1/R_y$ in Eqs. (19) are zero, but the twist $1/R_{xy}$ is present. The resulting configuration can be regarded as a flat plate subjected to uniform pretwist, having a twist angle ϕ at its free end. Results in Table 2 are for low aspect ratio ($a/b = 1$) blades having pretwist angles varying between 0 and 45°, with a width/thickness (b/h) ratio of 20 and Poisson's ratio (ν) of 0.3.

The analysis of Petricone and Sisto [33] was based upon helicoidal shell theory, and their numerical results were obtained by means of the Ritz method, using orthogonal polynomials as admissible functions.

Numerical results for the shell theory were typically obtained by taking $i, k = 1, 2, \cdots, 5$; $m = 2, 3, \cdots, 6$ and $j, l, n = 0, 2, 4$ (for symmetric modes) or $1, 3, 5$ (for antisymmetric modes) in Eqs. (23) yielding frequency determinants of 54th order in size. The convergence accuracy of the polynomials for twisted blades has been demonstrated previously [14]. Results for the beam theory were obtained by taking

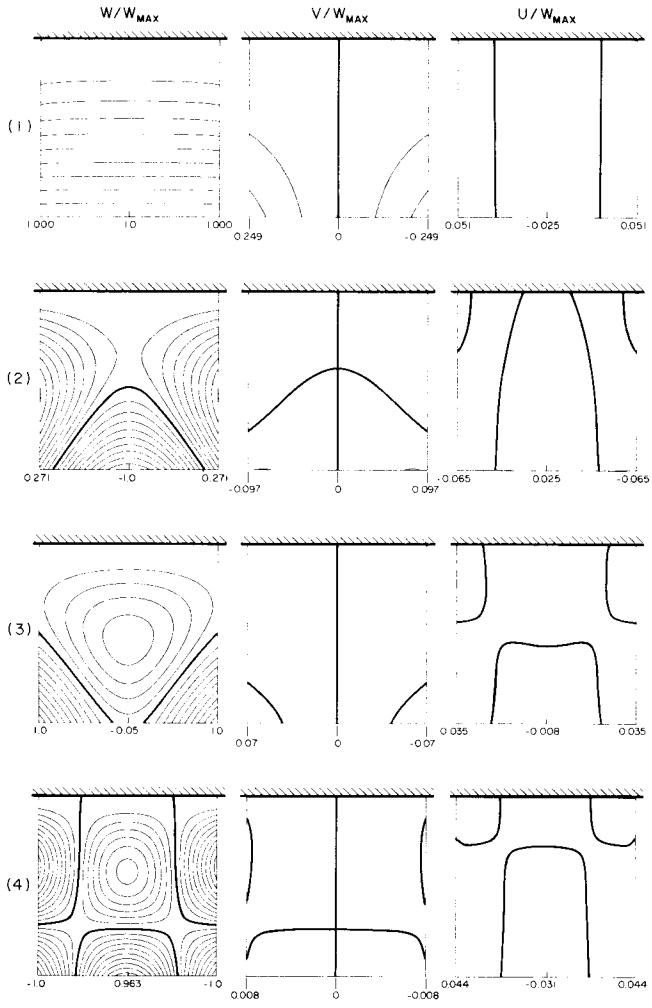

Figure 3 Symmetric mode shapes for a cambered blade ($b/h = 20$, $a/b = 1$, $b/R = 0.5$)

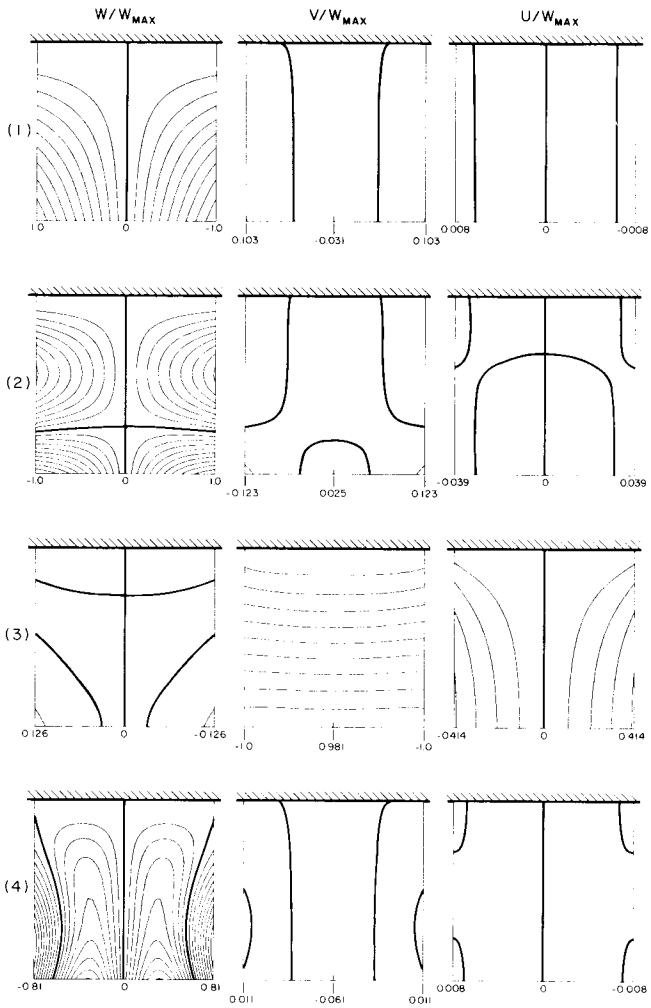

Figure 4 Antisymmetric mode shapes for a cambered blade ($b/h = 20$, $a/b = 1$, $b/R = 0.5$)

the first ten terms of the algebraic polynomials (14). No significant difference ($<4\%$) was found between the classical beam frequencies and those in Table 2, which include shear deformation and rotary inertia, except for sideways bending modes.

Nondimensional frequency parameters $\omega a^2\sqrt{\rho h/D}$ for the symmetric modes are listed in one half of Table 2. For a twisted plate the symmetric modes consist of coupled bending involving both v and w displacements (Fig. 2), uncoupled from the torsional modes, which are purely antisymmetric. For all twist angles given, the first two symmetric modes consist predominantly of w-displacements, and are similar to the first two spanwise bending modes of a beam. Table 2 indicates reasonable agreement among the results of shell and beam theories for these two modes. The third symmetric mode is chordwise bending (two mode lines nearly parallel to the length coordinate), which is missed by beam analysis. The fourth mode consists of sideways bending (i.e., predominantly v-displacements), not determined by Petricone and Sisto [33]. Detailed contour plots for the modes in the format of Fig. 3 are available [14] for the case $\phi = 30°$.

Considerable disagreement for the antisymmetric mode frequencies is observed in Table 2. For each twist angle, the first four antisymmetric modes consist of three torsional and one antisymmetric chordwise bending (i.e., three node lines essentially parallel to the length direction) modes. Beam theory results for the torsional modes are shown in the cases of neglecting warping constraint (without C_1) and including it (with C_1). When warping constraint is neglected the beam theory is observed to yield torsional frequencies which are typically low for small twist angles and too large for the higher modes at large twist angles. When warping constraint is included, the frequencies are all raised, giving good agreement with shell theory results for zero twist, but serious disagreements for $\phi = 20°$, $30°$ and $45°$. These trends can also be somewhat observed in the results of Carnegie comparing analysis with experiment ([3], Fig. 11), although the latter results were for large aspect ratio ($a/b = 6$) blades.

Beglinger and Schlachter [34] proposed a correction formula of the form

$$\frac{\omega^*}{\omega} = \left[1 + 2\zeta + \zeta^2\left\{1 + \left[\frac{\pi}{2}(2n-1)\right]^2\right\}\right]^{1/2} \qquad (25)$$

to account for torsional warping constraint, where n is the torsional mode number ($n = 1, 2, \cdots$) and

$$\zeta = \frac{1}{\ell}\sqrt{\frac{C_1}{C}} \qquad (26)$$

Table 2. Comparison of $\omega a^2\sqrt{\rho h/D}$ for Short, Twisted Blades ($a/b = 1$, $b/h = 20$, $\nu = 0.3$)

Twist angle, ϕ (degrees)	Mode number	Symmetric Modes: Present shell theory	Symmetric Modes: [33]	Symmetric Modes: Beam theory	Antisymmetric Modes: Present shell theory	Antisymmetric Modes: [33]	Antisymmetric Modes: Beam Theory Without C_1	Antisymmetric Modes: Beam Theory With C_1
0	1	3.474	——	3.347	8.513	——	6.430	8.474
	2	21.30	——	20.73	30.98	——	19.29	30.91
	3	27.20*	——	——	64.27†	——	——	——
	4	43.56**	——	42.91**	71.47	——	32.15	68.86
10	1	3.453	3.48	3.344	9.509	9.58	7.949	9.943
	2	21.10	21.4	20.38	31.66	32.8	23.85	34.76
	3	27.19*	27.8	——	64.36†	——	——	——
	4	44.25**	——	43.39**	71.76	——	39.74	73.56
20	1	3.387	3.47	3.336	12.16	12.0	11.34	13.24
	2	20.48	20.6	19.46	33.72	35.2	34.03	43.82
	3	27.32*	27.6	——	64.65†	——	——	——
	4	46.19**	——	44.58**	72.71	——	56.72	85.82
30	1	3.265	3.48	3.322	16.08	15.0	15.42	17.23
	2	19.41	19.6	18.21	37.35	37.8	46.27	55.11
	3	27.94*	27.9	——	65.21†	——	——	——
	4	49.04**	——	45.89**	74.58	——	77.11	102.4
45	1	2.939	3.51	3.294	24.35	19.3	21.99	23.71
	2	17.18	18.0	16.19	46.45	42.6	65.96	73.77
	3	30.56*	28.6	——	66.96†	——	——	——
	4	52.46**	——	45.56**	80.44	——	109.9	131.3

* Chordwise bending mode

** Sideways bending mode

†Antisymmetric chordwise bending mode

with ℓ being the beam length, and C and C_1 being the torsional rigidity and warping restraint factors, respectively, as used previously in Eq. (4). For the twisted plate having a rectangular cross-section

$$\zeta = \frac{b}{\ell}\sqrt{\frac{1+\nu}{24}} \qquad (27)$$

and letting $b/\ell = 1$ and $\nu = 0.3$ the right hand side of Eq. 25 becomes 1.286, 1.650 and 2.205 for $n = 1$, 2 and 3 respectively. Applying these correction factors to the torsional frequencies listed in Table 2 for $\phi = 0$ yields 8.269, 31.83 and 70.89, which are seen to compare reasonably with the frequencies both of shell theory and of beam theory (with C_1). However, a cursory inspection of Table 2 also shows that the same factors applied to the beam frequencies for non-zero angles of twist result in large over-corrections to the beam frequencies.

It should be noted that a twist angle of zero degrees in Table 2 yields a flat plate which would be identical to the cambered blade of Table 1 having $b/R = 0$. Sideways bending modes are symmetric for twisted blades and antisymmetric for cambered blades.

Another set of twisted blades for which both theoretical and experimental results are available is that studied by MacBain [35]. This set consisted of thin ($b/h = 33.4$) plates of moderate aspect ratio ($a/b = 2.33$) pretwisted through various tip angles ($\phi = 0, 12, 17, 23.5, 30$ and 38 degrees). MacBain obtained numerical results using the NASTRAN finite element program with 1265 degrees of freedom [36] and compared them with data resulting from tests using holography. Frequency parameters $\omega a^2\sqrt{\rho h/D}$ for the plate ($b/R_y = 0$) having a moderate pretwist angle ($\phi = 30°$) are presented in Table 3, and compared there with the corresponding results [14] from the present shallow shell theory and with beam theory (including shear deformation and rotary inertia).

As found previously for blades having little or no camber (cf. Table 2), the spanwise bending mode frequencies given in Table 3 for beam theory are seen to be typically somewhat low, because the beam model does not recognize the additional stiffening capability of sideways bending moments M_y induced by Poisson effects. Again the antisymmetric, torsional mode frequencies are predicted somwhat low by beam theory for the fundamental (1A) mode and become too high for higher modes when warping restraint is not accounted for. Including warping constraint (values given in parentheses) results in appropriate correction for the first torsional frequency, but raises the third one to an unacceptable level. But, on the whole, the beam theory results for MacBain's twisted plate are seen to be reasonably acceptable, at least for the first seven modes.

The second part of the Table 3 shows the effects of adding a small amount of camber $b/R_y = 0.215$, or $a/R_y = 0.5$ to the MacBain twisted blade. Generally, the frequencies are increased slightly, but the beam theory results are now seen to deviate considerably from those of the shallow shell theory. In this case the modes involve complete coupling between the bending in two directions and torsion, compared with the uncambered blade which has torsion uncoupled. The magnitude of the coupling can be seen from previously presented mode shapes [14] (somewhat further complicated by the addition of rotational effects).

CONCLUSIONS

Beam theory is generally inadequate to determine the the free vibration frequencies and mode shapes of moderate to low aspect ratio turbomachinery blades. It may also be inadequate for large aspect ratio blades if a careful dynamic response analysis is to be made, requiring reasonably accurate knowledge of the first ten or more frequencies and mode shapes.

The inadequacy of beam theory is seen in the following ways:

1. Modes which are predominantly chordwise bending are completely missed while others involving significant amounts of chordwise

Table 3. Comparison of $\omega a^2\sqrt{\rho h/D}$ for Moderate Aspect Ratio ($a/b = 2.33$), Twisted ($\phi = 30°$), Thin ($b/h = 33.4$) Blades.

b/R_y	Type of results	$\omega a^2\sqrt{\rho h/D}$							
	Mode	1S	2S	1A	3S	2A	4S*	5S	3A
0	Present shell theory	3.237	19.46	30.96	57.81	86.60	109.2	124.7	135.2
	Finite element [35]	3.473	19.56	28.99	57.38	82.08	88.74	116.1	129.3
	Experiment [35]	3.39	19.09	27.54	57.84	76.87	100.2	115.0	123.6
	Beam theory	3.358	18.79	27.80	55.90	83.41	104.9	120.3	139.0
	(with C_1)			(29.48)		(90.63)			(158.0)
	Mode number	1	2	3	4	5	6	7	8
0.215	Present shell theory	3.660	20.99	31.95	60.61	90.74	109.4	122.6	135.0
	Beam theory	4.574	25.48	27.73	75.48	83.11	111.8	138.5	155.1
	(with C_1)	(4.574)	(25.49)	(29.40)	(75.48)	(90.32)	(111.8)	(155.2)	(157.4)

*Sideways bending mode

bending are poorly determined.

2. Frequencies of modes which are essentially either spanwise bending or torsion may be poorly estimated, especially for blades of low aspect ratio, because of other limitations in the analytical model.
3. Typical blades with no symmetry may have strong coupling between all types of spanwise and chordwise bending and torsion, making suitable corrections for above mentioned limitations difficult.

Inaccuracies in the spanwise bending frequencies may be due to any or all of the following:

1. Additional stiffness due to chordwise bending moments induced by Poisson effects.
2. Difficulty in determining a proper shear correction factor to utilize with the shear deformatin theory.
3. The constraint that "plane cross-sections remain plane", required by both classical and shear deformation beam theories, which ignores additional flexibility due to cross-sectional warping.

The last factor was seen to be particularly important, especially for low aspect ratio blades, and is not considered in any beam model of blade vibrations known to the writers.

Large inaccuracies in the torsional frequencies may arise because of:

1. The constraint on cross-sectional warping due to a fixed root.
2. Inaccuracy in representing additional beam stiffness due to pretwist.

Much of the above-mentioned inaccuracy in representing the spanwise bending and torsional modes could be eliminated by incorporation of proper correction factors determined from solutions of the classical theory of elasticity.

By contrast the shallow shell theory is straightforwardly applied and is capable of representing all the vibration modes accurately. The theory is capable of considerable generalization beyond that used in the present work in order to represent actual turbomachinery blades more accurately. The generalizations include:

1. Elastic root constraint.
2. Attached shrouds.
3. Thick shell theory, for thicker blades.
4. A deeper "shallow" shell theory (including more terms in the strain-displacement equations, but still relating all equations to the projected base plane.), for more highly cambered and/or twisted blades.
5. Accurate representation of rotational effects, including Coriolis forces.
6. Variable thickness and curvature.
7. Nonrectangular blade planforms.
8. Anisotropic and/or nonhomogeneous materials such as composites.
9. Accurate determination of initial stresses due to rotation, as well as vibratory stresses.
10. Structural damping or layered damping treatments.

But the one-dimensional beam theory has an important advantage over the two-dimensional shell theory for blades and vibration modes that it is capable of representing; namely, it can do so with fewer degrees of freedom, thus requiring less computer time. Similarly, the shell theory approach has been shown to require significantly less degrees of freedom [12] than finite element models, for the same degree of accuracy. Thus, both approaches have their proper places in blade vibration analysis, particularly in preliminary design where the effects of changing parameters need to be studied.

ACKNOWLEDGEMENTS

The authors wish to acknowledge the help of Mr. A.J. Wang in obtaining numerical results for the shell analysis. This work was partially supported by the National Aeronautics and Space Administration, Lewis Research Center, under Grant No. NAG 3-36.

REFERENCES

1. Leissa, A., "Vibrational Aspects of Rotating Turbo-machinery Blades", Applied Mechanics Reviews, Vol. 34, No. 5, 1981, pp. 629-635.

2. Carnegie, W., "Static Bending of Pre-Twisted Cantilever Blades", Proceedings of the Institution of Mechanical Engineers, Vol. 171, No. 32, 1957, pp. 873-894.

3. Carnegie W., "Vibrations of Pre-Twisted Cantilever Blading", Proceedings of the Institution of Mechanical Engineers, Vol. 173, No. 12, 1959, pp. 343-374.

4. Carnegie, W., "Vibrations of Rotating Cantilever Blading: Theoretical Approaches to the Frequency Problem Based on Energy Methods", Journal Mechanical Engineer-Science, vol. 1, No. 3, 1959, pp. 235-240.

5. Carnegie, W., "Vibrations of Pre-Twisted Cantilever Blading: An Additional Effect Due to Torsion", Proceedings of the Institution of Mechanical Engineers, Vol. 176, No. 13, 1962, pp. 315-322.

6. Carnegie, W., "Vibrations of Pre-Twisted Cantilever Blading Allowing for Rotary Inertia and Shear Deflection", Journal Mechanical Engineering Science, Vol. 6, No. 2, 1964, pp. 105-109.

7. Carnegie, W., "A Note on the Application of the Variational Method to Derive the Equations of Dynamic Motion of a Pre-Twisted Cantilever Blade Mounted on the Periphery of a Rotating Disc Allowing for Shear Deflection, Rotary Inertia and Torsion Bending", Bulletin of Mechanical Engineering Education, Vol. 5, 1966, pp. 221-223.

8. Carnegie, W., "The Application of the Variational Method to Derive the Equations of Motion of Vibrating Cantilever Blading under Rotation", Bulletin of Mechanical Engineering Education, Vol. 6, 1967, pp. 29-38.

9. Houbolt, J.C. and Brooks, G.W., "Differential Equations of Motion for Combined Flapwise Bending, Chordwise Bending and Torsion of Twisted Non-uniform Rotor

Blades", NACA Report 1346, 1958.
10. Montoya, J., "Coupled Bending and Torsional Vibrations in a Twisted, Rotating Blade", Brown Boveri Review, Vol. 53, No. 3, 1966, pp. 216-230.
11. Leissa, A.W., "Vibrations of Turbine Engine Blades by Shell Analysis", Shock and Vibration Digest, Vol. 12, No. 11, 1980, pp. 3-10.
12. Leissa, A.W., Lee, J.K. and Wang, A.J., "Rotating Blade Vibration Analysis Using Shells", ASME Paper No. 81-GT-80, Journal of Engineering for Power (to appear).
13. Leissa, A.W., Lee, J.K. and Wang, A.J., "Vibrations of Cantilevered Shallow Cylindrical Shells Having Rectangular Planform", Journal of Sound and Vibration (to appear).
14. Leissa, A.W., Lee, J.K. and Wang, A.J., "Vibrations of Twisted Rotating Blades", ASME Paper No. 81-DET, to be presented at the ASME Vibrations Conference, Hartford, Conn., Sept. 1981 and to be published in the Journal of Mechanical Design.
15. Timoshenko, S.P. and Goodier, J.N., Theory of Elasticity, Third Edition, McGraw-Hill, Inc., 1970.
16. Timoshenko, S.P., "On the Correction for Shear of the Differential Equations for Transverse Vibrations of Prismatic Bars", Philosophical Magazine, Ser 6, Vol. 41, 1921, p. 742.
17. Carnegie, W., "Experimental Determination of the Centre-of-Flexure and Centre-of-Torsion Co-ordinates of an Asymmetrical Aerofoil Cross-Section", Journal Mechanical Engineering Science, Vol. 1, No. 3, 1959, pp. 241-249.
18. Carnegie, W., Stirling, C. and Fleming, J., "Vibration Characteristics of Turbine Blading Under Rotation - Results of an Initial Investigation and Details of a High-Speed Test Installation", Proceedings of the Institution of Mechanical Engineers, Vol. 180, Part 31, 1966.
19. Carnegie, W., Dawson, B. and Thomas, J., "Vibration Characteristics of Cantilever Blading", Proceedings of the Institution of Mechanical Engineers, Vol. 180, Part 31, 1966, p. 71.
20. Carnegie, W. and Dawson, B., "Vibration Characteristics of Straight Blades of Asymmetrical Aerofoil Cross-Section", Aeronautical Quarterly, Vol. 20, 1969, pp. 178-190.
21. Rao, J.S. and Carnegie, W., "Solution of the Equations of Coupled-Bending Bending Torsion Vibrations of Turbine Blades by the Method of Ritz-Galerkin", International Journal of Mechanical Sciences, Vol. 12, 1970, pp. 875-882.
22. Carnegie, W., and Dawson, B., "Vibration Characteristics of Pre-Twisted Blades of Asymmetrical Aerofoil Cross-Section", Aeronautical Quarterly, Vol. 22, 1971, pp. 257-273.
23. Carnegie, W. and Thomas, J., "The Effects of Shear Deformation and Rotary Inertia on the Lateral Frequencies of Cantilever Beams in Bending", ASME Journal of Engineering for Industry, 1972, pp. 267-278.
24. Rao, J.S., "Natural Frequencies of Turbine Blading - A Survey", Shock and Vibration Digest, Vol. 5, No. 10, 1973, pp. 3-16.
25. Rao, J.S., "Turbine Blading Excitation and Vibration", Shock and Vibration Digest, Vol. 9, No. 3, 1977, pp. 15-22.
26. Rao, J.S., "Turbomachine Blade Vibration", Shock and Vibration Digest, Vol. 12, No. 2, 1980, pp. 19-26.
27. Goldenveizer, A.L., "Theory of Elastic Thin Shells", English Translation, Pergamon Press (1961).
28. Novozhilov, N.V., The Theory of Shells (English Translation), P. Noordhoff Ltd., Groningen, The Netherlands, 1959.
29. Leissa, A.W., Vibration of Shells, NASA SP-288, U.S. Government Printing Office, 1973.
30. Subrahmanyam, K.B., Kulkarni, S.V. and Rao, J.S., "Coupled Bending-Torsion Vibrations of Rotating Blades of Asymmetric Aerofoil Cross Section with Allowance for Shear Deflection and Rotary Inertia by Use of the Reissner Method", Journal of Sound and Vibration, Vol. 75, No. 1, 1981, pp. 17-36.
31. Leissa, A.W., Vibration of Plates, NASA SP-160, U.S. Government Printing Office, 1969.
32. Leissa, A.W., "The Free Vibrations of Rectangular Plates", Journal of Sound and Vibration, Vol. 31, No. 3, 1973, pp. 257-293.
33. Petricone, R.D. and Sisto, F., "Vibration Characteristics of Low Aspect Ratio Compressor Blades", Journal of Engineering for Power, Trans. ASME, Vol. 93, No. 1, 1971, pp. 103-112.
34. Beglinger, V. and Schlachter, W., "Influence of Support Elasticity, Shear Deformation, Rotary Inertia and Cross-Sectional Warping on the Natural Frequencies of Turbomachine Blades", Sulzer Technical Review, Research Number 1978, 1978, pp. 19-26.
35. MacBain, J.C., "Vibratory Behavior of Twisted Cantilever Plates", Journal of Aircraft, Vol. 12, No. 4, 1975, pp. 343-349.
36. MacBain, J.C., Private Communication, April, 1981.